Available online at www.sciencedirect.com
SCIENCE DIRECT®
Journal of Catalysis 228 (2004) 321–332
JOURNAL OF CATALYSIS
www.elsevier.com/locate/jcat

Characterization and catalytic properties of cobalt supported on delaminated ITQ-6 and ITQ-2 zeolites for the Fischer–Tropsch synthesis reaction

Patricia Concepción [a], Carlos López [a], Agustín Martínez [a,*], Víctor F. Puntes [b]

[a] *Instituto de Tecnología Química, UPV-CSIC, Avenida de los Naranjos s/n, 46022 Valencia, Spain*
[b] *Departament de Física Fonamental, Universitat de Barcelona, Spain*

Received 25 June 2004; revised 2 September 2004; accepted 6 September 2004

Available online 22 October 2004

Abstract

Cobalt catalysts (ca. 20 wt% Co) supported on all-silica delaminated ITQ-2 and ITQ-6 zeolites have been prepared by impregnation with aqueous $Co(NO_3)_3$ solutions. The catalysts have been characterized by X-ray diffraction (XRD), nitrogen adsorption, transmission electron microscopy (TEM), temperature-programmed reduction (TPR), and infrared spectroscopy of adsorbed CO. The catalytic properties for the Fischer–Tropsch synthesis (FTS) reaction under typical FTS conditions (493 K, 20 bar, $H_2/CO = 2$) have been evaluated, and the results compared with those obtained over a conventional Co/SiO_2 and a mesoporous Co/MCM-41 catalyst with comparable cobalt loading. Co/ITQ-6 was the most active catalyst, with a FTS reaction rate which was about 1.5 and 1.8 times higher than that of Co/MCM-41 and Co/SiO_2, respectively. The high activity of Co/ITQ-6 is ascribed both to a relatively good dispersion (as observed by TEM) and to a high reducibility (determined by TPR) of the supported Co_3O_4 particles. The dispersion and reducibility of cobalt particles in Co/ITQ-2 were very close to those in Co/SiO_2. Consequently, both catalysts presented similar FTS reaction rates. In addition, Co/ITQ-6 and Co/ITQ-2 presented a higher selectivity toward the formation of C_{5+} hydrocarbons than Co/SiO_2 and Co/MCM-41. The higher C_{5+} selectivity of the catalysts based on the delaminated zeolites was ascribed to a higher concentration of coordinatively unsaturated Co^0 sites which are characterized by a band at 1897 cm^{-1} in the infrared spectrum of adsorbed CO. This type of site having an enhanced electron density might stabilize surface hydrocarbon intermediates favoring chain growth processes.

Keywords: Cobalt catalyst; Fischer–Tropsch synthesis; Mesoporous MCM-41; Delaminated zeolites; ITQ-2; ITQ-6

1. Introduction

The production of synthetic fuels, and particularly middle distillates, from natural gas through the Fischer–Tropsch synthesis (FTS) process has received renewed interest in the last years [1,2]. Among the different factors contributing to this are the limited crude reserves and the decreasing trend in the quality of the supplied oil, the vast reserves of natural gas, the growing demand for middle distillates, the tighter fuel specifications, and the excellent quality of the synthetic distillates. Moreover, recent improvements achieved in the gas-to-liquid (GTL) technology making these processes more efficient and cost competitive must also considered [3–6]. In particular, diesel fuels produced by the FTS process offer significant advantages over those derived from crude oil, as they are mainly formed by sulfur-free linear paraffins possessing high cetane numbers (typically above 70) [7].

Cobalt-based FTS catalyst are preferred over Fe-based systems for producing synthetic diesel fuels, since they favor the formation of long-chain *n*-paraffins, are more stable against deactivation by water (a by-product of the FTS reaction), are less active for the competitive water gas-shift (WGS) reaction, and produce less oxygenates [8–10]. Typ-

* Corresponding author. Fax: +34 96 3877809.
E-mail address: amart@itq.upv.es (A. Martínez).

0021-9517/$ – see front matter
doi:10.1016/j.jcat.2004.09.011

ically, the preparation of Co-based FTS catalysts involves the impregnation of a cobalt precursor salt over a porous inorganic solid, followed by calcination and reduction. Typical supports used for dispersing cobalt in FTS catalysts are amorphous SiO_2, Al_2O_3, and to a lesser extent TiO_2 [11]. According to Iglesia and co-workers [12,13], the FTS activity of supported Co catalysts under conditions favoring high C_{5+} selectivity, is proportional to the concentration of surface Co^0 sites (i.e., the turnover of Co^0 is constant) irrespective of the nature of the support used. Reuel and Barthlomew [14], however, found that turnover frequencies of supported Co catalysts decreased with cobalt dispersion. This effect was ascribed either to changes in the surface structure or to stronger cobalt-support interactions with decreasing particle size. Moreover, catalysts with a high density of surface Co^0 sites were seen to favor the formation of high molecular weight *n*-paraffins [13], which are desired for maximizing the production of diesel-range hydrocarbons. For a given cobalt loading, the number of surface Co^0 sites in the reduced catalysts will mainly depend on two parameters, the dispersion and the reduction degree of the supported cobalt oxide particles [12,15]. These two parameters are determined, to a great extent, by the cobalt–support interaction strength [16]. A strong Co–support interaction, as it occurs in the case of Al_2O_3 and TiO_2, favors the dispersion of the supported Co particles, but at the same time decreases their reducibility [17], leading to catalysts with a limited number of accessible Co^0 sites. On the contrary, a much weaker interaction leading to a higher Co reducibility occurs for Co/SiO_2 catalysts, but in this case the cobalt particles tend to agglomerate on the silica surface during the thermal activation treatments resulting in a relatively low metal dispersion, and thus, a low number of surface active sites. The reducibility of supported cobalt oxide may be increased by the addition of small amounts of noble metals, such as Pt, Pd, Re, or Ru [12,17,18]. Transition metals, such as Mn and Zr [17,19,20], have also been used as promoters to improve the dispersion of the supported cobalt particles.

Recently, ordered mesoporous silicas of the MCM and SBA type having high surface area and a narrow pore-size distribution have been used as supports for preparing Co-based FTS catalysts with the aim of improving Co dispersion by confining the cobalt particles inside the mesoporous channels [20–26]. The properties of the cobalt particles were greatly affected by the pore size of the mesoporous support. Thus, an increase of the average particle size of the supported Co oxide phase was found with increasing the pore size of the periodic mesoporous silica [21,22]. Larger cobalt particles sizes formed in wider pore mesoporous supports, such as SBA-15, were more reducible and lead to catalysts with higher catalytic activity and lower methane selectivity than smaller particles in narrower pore materials, such as MCM-41. An increase in the mean crystallite size and reducibility of cobalt particles with increasing the average pore size has also been observed for a series of Co/SiO_2 catalysts prepared from commercial amorphous silicas with

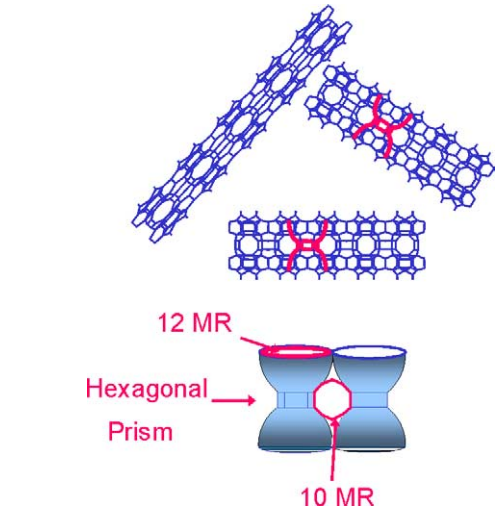

(a) ITQ-2

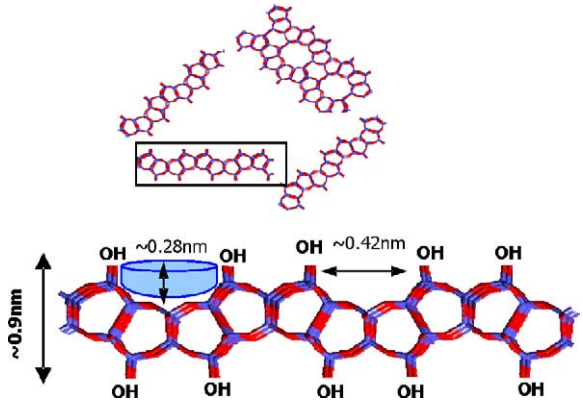

(b) ITQ-6

Fig. 1. Schematic representation of the (a) ITQ-2 and (b) ITQ-6 structures.

varied pore diameters [27]. These authors found an optimum FTS activity and C_{5+} selectivity for a silica having an average pore diameter of 10 nm. We have recently reported that, at comparable Co loadings, Co/SBA-15 samples prepared from a SBA-15 mesoporous silica with an average pore size of 10 nm were significantly more active than conventional Co/SiO_2 catalysts owing to an improved Co dispersion [20].

Recently, two new zeolitic materials, ITQ-2 and ITQ-6, have been synthesized in our laboratories [28–30]. ITQ-2 and ITQ-6 zeolites were obtained by delamination of layered zeolite precursors having the MWW (MCM-22) and FER (ferrierite) structure, respectively. The delaminated zeolites are mostly formed by single zeolitic layers organized in a "house of card"-type structure having a very high external surface area, usually above 600 m^2/g, typically observed for ordered mesoporous materials. A significant difference, however, between the delaminated zeolites and the mesoporous MCM-41 and SBA-type materials is that the former have short-range order owing to the zeolitic nature of the layers, and thus are more thermal and hydrothermally stable. A schematic representation of the ITQ-2 and ITQ-6 structures is shown in Fig. 1. ITQ-2 consists of thin sheets 2.5 nm in height presenting an hexagonal array of

"cups" (0.7 × 0.7 nm) that penetrate into the sheet from both sides connected by a double 6-member ring (MR) window (Fig. 1a). The sheets contain a circular 10-MR sinusoidal channel system. The external surface of ITQ-6 contains cups delimited by 10-MR and are thus of a smaller diameter than the 12-MR delimited cups of ITQ-2, as seen in Fig. 1b. Moreover, the ITQ-6 layers do not contain 10-MR channels.

The singular structure of the delaminated zeolites, and particularly the very high and well-defined external surface area, makes these materials attractive to be used as supports for dispersing active metal phases. In this sense, NiMo and Pt catalysts supported on (Al)-ITQ-2 were applied for hydrocracking of vacuum gas oil and hydrogenation of aromatics with promising results [31]. Therefore, in this work we have studied the possibilities of using pure silica delaminated ITQ-2 and ITQ-6 zeolites as supports for preparing cobalt-based Fischer–Tropsch catalysts. The materials have been characterized by N_2 adsorption, X-ray diffraction (XRD), transmission electron microscopy (TEM), temperature-programmed reduction (TPR), and infrared spectroscopy of adsorbed CO (IR-CO). The activity and selectivity for the FTS reaction were evaluated under typical hydrocarbon synthesis conditions (493 K and 20 bar), and the results compared with a mesoporous Co/MCM-41 and a conventional Co/SiO_2 sample with equivalent Co loading.

2. Experimental

2.1. Preparation of catalysts

Pure silica ITQ-2 zeolite was obtained by swelling the layered MWW zeolite precursor in cetyltrimethylammonium bromide (CTABr) as described in [29]. Typically, 27 g of precursor is mixed with 105 g of an aqueous solution of CTABr (29 wt%) and 33 g of an aqueous solution of tetrapropylammonium hydroxide (TPAOH, 40 wt%), and the resulting solution is refluxed for 16 h at 353 K. The layers are forced apart by placing the slurry in an ultrasound bath (50 W, 40 kHz) for 1 h. Separation of the solids is done by acidification of the medium with concentrated hydrochloric acid (HCl, 37%) until the pH is below 2, followed by centrifugation. Calcination of the material at 813 K yields ITQ-2.

An all-silica ITQ-6 sample was prepared by a similar procedure by swelling the laminar precursor of ferrierite (PREFER) according to the procedure described in [28]. Typically, 10 g of an aqueous solution of PREFER (20 wt%) is mixed with 8 g of an aqueous solution of CTABr (25 wt%) and 10 g of an aqueous solution of TPAOH (40 wt%). After vigorous stirring at 398 K, the PREFER was swelled in CTABr and TPAOH. Separation of the layers is achieved by sonication, acidification, and centrifugation under the same conditions described above for ITQ-2. After washing and drying the solid, the ITQ-6 zeolite is obtained by calcination at 853 K to remove the organic material.

For comparison purposes, a mesoporous silica MCM-41 sample and a commercial amorphous SiO_2 (Fluka, silica gel 100) were also used as supports. The MCM-41 sample was synthesized from Aerosil-200 (Degussa) as silica source, tetramethylammonium hydroxide (TMAOH, Aldrich), and hexadecyltrimethylammonium bromide (CTMABr, Aldrich) as the surfactant template, following the procedure reported in [32]. Thus, a gel of the following molar composition,

$$SiO_2{:}0.26\ CTABr{:}0.40\ TMAOH{:}29\ H_2O$$

was loaded in Teflon-lined stainless-steel autoclaves and heated in static at 408 K for 24 h. The resulting solid was washed with distillate water and dried at 333 K overnight. Finally, the organic was removed by calcination at 813 K in flowing N_2 for 1 h and then with air at the same temperature for 5 h, yielding the MCM-41 material.

Incorporation of cobalt was accomplished by impregnation of the respective supports with an excess of an aqueous solution containing the required amount of $Co(NO_3) \cdot 6H_2O$ (Aldrich, 98%) to achieve a nominal concentration of 20 wt% cobalt in the final catalysts. The volume of the impregnating solution used was six times the volume required to fill the pores of the support. After stirring for 1 h at room temperature, the solvent was eliminated by rotavaporation, and the solid was further dried at 333 K for 12 h. In the case of MCM-41, the cobalt salt was dissolved in ethanol for preparing the impregnating solution. Finally, all Co-supported catalysts were calcined in a muffle oven at 573 K for 10 h.

2.2. Characterization techniques

The cobalt content in the calcined catalysts was determined by atomic absorption spectrophotometry (AAS) in a Varian Spectra A-l0 Plus apparatus.

Textural properties of the supports and Co-containing catalysts were obtained from the nitrogen adsorption isotherms determined at 77 K in a Micromeritics ASAP 2000 equipment. Surface areas were calculated by the BET method and the pore-size distributions were obtained using the BJH formalism. Prior to the adsorption measurements the samples were outgassed at 473 K for 24 h.

X-ray diffraction was used to identify the nature of the crystalline cobalt oxide phases. XRD patterns were obtained at room temperature in a Philips X'pert diffractometer using monochromatized Cu $K\alpha$ radiation.

The Co_3O_4 particle-size distribution and the average cobalt particle diameter in the oxidized samples were obtained by dark-field transmission electron microscopy in an Hitachi 800MT microscope operated at an accelerating voltage of 200 kV. Dark field consists of observing the image produced by the diffracted electrons corresponding to a determined lattice spacing leaving the rest dark. In detail, to obtain the size distribution of the cobalt particles, the diameter of the equivalent circle which encloses the bright spots in the dark-field images was measured. Between 100 and

300 particles coming from at least 10 different blind-coded images were measured. Unfocused or superimposed particles were discarded. From these data, the statistical average was calculated. For observation the samples were grounded to a fine powder and diluted in ethanol to give a 1:3 volume ratio and sonicated for 2 min. A Cu grid covered with a thin film of amorphous carbon was dipped in the methanol slurry and then allowed to dry. The average Co_3O_4 particle sizes obtained were then converted to the corresponding cobalt metal diameters in reduced catalysts by considering the relative molar volumes of Co^0 and Co_3O_4 by using the following equation [33]:

$$d(Co^0) = 0.75\, d(Co_3O_4).$$

Then, Co^0 metal dispersions were estimated from the mean Co^0 particle sizes assuming a spherical geometry of the metal particles with uniformly site density of 14.6 atoms/nm^2 using the following equation [33,34],

$$D = 96/d,$$

where D is the percentage dispersion and d is the mean particle size of Co^0 in nanometers.

The reduction behavior of the supported oxidized cobalt phases was studied by temperature-programmed reduction in a Micromeritics Autochem 2910 equipment. About 30 mg of the calcined catalyst was initially flushed with 30 cm^3/min of Ar at room temperature for 30 min and then a mixture of 10 vol% of H_2 in Ar was passed through the catalyst at a total flow rate of 50 cm^3/min while the temperature is increased up to 1173 K at a heating rate of 10 K/min. The H_2 consumption rate was monitored in a thermal conductivity detector (TCD) previously calibrated using the reduction of CuO as reference.

A different set of experiments was performed in the same equipment to determine the extent of cobalt reduction after submitting the calcined samples to the same reduction treatment applied prior the catalytic tests. For this purpose, about 100 mg of oxidized catalyst was placed in the TPR cell and reduced in situ at 673 K for 10 h at a heating rate of 1 K/min by flowing 50 cm^3/min of a mixture of 10 vol% H_2 in Ar. Then, the temperature was increased from 673 to 1173 K at a rate of 10 K/min and the H_2 consumption registered. The degree of Co reduction was then calculated from the amount of H_2 consumed assuming that complete reduction of Co_3O_4 to CoO and partial reduction of CoO to Co^0 took place during the in situ reduction treatment at 673 K. This assumption is based on the fact that supported Co_3O_4 crystallites have been shown to be reduced to CoO at temperatures typically below 673 K, while higher temperatures are needed to reduce CoO to metallic cobalt [17]. According to the stoichiometry of the second reduction step, the moles of H_2 consumed will be equivalent to the moles of cobalt which remain unreduced after the in situ reduction step at 673 K:

$$CoO + H_2 \rightarrow Co^0 + H_2O.$$

Then, the degree of reduction (DR) is calculated by applying the following equation:

$$\mathrm{DR}\ (\%) = \left[1 - (n_{H_2})/(n_{Co})\right] \times 100,$$

where n_{H_2} is the moles of H_2 consumed and n_{Co} is the moles of total cobalt in the catalyst.

The nature of cobalt species in the different supports was studied by infrared spectroscopy with adsorbed CO on a Bio-Rad FTS-40A spectrometer using a quartz infrared cell fitted with KRS-5 windows and an external furnace. Prior to the CO adsorption experiments the catalysts were reduced ex situ in pure hydrogen flow at 673 K for 10 h. The samples were pressed into wafers (10 mg/cm^2) and reduced again in the IR cell under static conditions at 623 K in order to avoid the presence of oxidized surface species that might be formed in contact with air during the transfer of the samples from the ex situ reduction reactor to the spectrometer. After the in situ reduction treatment the samples were cooled in vacuum and then pulses of CO were introduced at 298 K using calibrated volumes (1.55 cm^3).

2.3. Catalytic experiments

The Fischer–Tropsch synthesis reaction was performed in a downflow fixed-bed stainless-steel reactor ($d_i = 10$ mm, $l = 40$ cm). Typically, the reactor was loaded with 1.0 g of catalyst (0.25–0.42 mm particle size) diluted with silicon carbide (0.25–0.59 mm particle size) up to a constant volume of 6.4 cm^3. Prior to the catalytic experiments the catalysts were reduced in situ at atmospheric pressure by increasing the temperature at a heating rate of 1 K/min from ambient to 673 K and maintained at this temperature for 10 h while passing a flow of pure hydrogen (400 cm^3/min) through the reactor. After the reduction step the temperature was lowered to 373 K under a flow of H_2 and then a mixture of H_2, CO, and Ar (internal standard) in a volume ratio of 6:3:1 ($H_2/CO = 2$) was fed at a total flow rate of 250 cm^3/min, corresponding to a gas hourly space velocity (GHSV) of 13.5 L(NTP)/(g_{cat} h) referred to the syngas mixture. Then, the reactor pressure was slowly increased to 20 bar, and the temperature in the catalyst bed was raised from 373 to 493 K at a heating rate of 4 K/min. Once the reaction temperature of 493 K was achieved, which is considered as time zero (TOS = 0), the reaction was led to proceed during a period of 15–20 h to ensure stabilization of the catalyst activity. During the reaction the temperature in the catalyst bed was controlled to 493 K ($\pm$ 1 K) by means of two independent heating zones with the corresponding temperature controllers connected to thermocouples located in different positions inside the catalytic bed. Preliminary experiments were carried out to ascertain that under these conditions the reaction was not controlled by external nor intraparticle mass-transfer limitations.

During the reaction, the effluent leaving the reactor passed through a hot trap kept at 473 K and at the system pressure (20 bar) to collect the waxy products, and the

stream of products exiting the trap (unreacted H_2 and CO, Ar, CO_2, water, alcohols, and hydrocarbons up to about C_{20}) was depressurized and analyzed on line at periodic intervals by gas chromatography in a Varian 3800 chromatograph equipped with three columns and two detectors. Analysis of Ar (reference gas), CO, CO_2, and CH_4 was performed using two packed columns, a Porapak Q (0.5 m length) and a 13X molecular sieve (1.5 m length), and a thermal conductivity detector. Alcohols and hydrocarbons from C_1 up to about C_{20} were analyzed using a capillary column (WCOT fused silica, 2.5 m length) and a flame ionization detector (FID). To avoid condensation of the heaviest hydrocarbons, a controlled flow of nitrogen (50 cm^3/min) was added to the product stream after depressurization while all transfer lines between the reactor and GC were kept at a temperature of 473 K.

3. Results and discussion

3.1. Catalyst characterization

3.1.1. Structural and textural properties of materials

The X-ray diffraction patterns of calcined ITQ-2 and ITQ-6 zeolites are shown in Fig. 2. As observed, ITQ-2 does not show the 00*l* peaks with the 2.5-nm periodicity typical of the MWW topology, indicating a reduction of long-range order along the *c* axis. Similarly, the diffractogram of ITQ-6 shows a strong reduction of the intensity of the reflexions corresponding to planes (*h*00) as compared to the XRD pattern of ferrierite (not shown), indicating a remarkable loss of order along the *a* axis. These structural changes are in agreement with the proposed structures (Fig. 1) in which the materials are mostly formed by single layers of the corresponding lamellar precursors. The X-ray diffractogram of the calcined MCM-41 sample (insert in Fig. 2) shows the characteristic (*100*) sharp reflection at low angles ($2\theta \approx 2.4°$), and the less intense (*110*), (*200*), and (*210*) reflections at higher angles, which is indicative of a highly ordered mesoporous structure.

The N_2 adsorption isotherms for ITQ-2, ITQ-6, and MCM-41 samples are shown in Fig. 3. The isotherm of MCM-41 presents a sharp inflection at a relative pressure of about 0.25, indicating a narrow distribution of pores in the mesopore range characteristic for this material. The mean pore diameter of MCM-41 calculated by the BJH method is 3.1 nm. On the other hand, the shape of the adsorption isotherms for the delaminated ITQ-2 and ITQ-6 zeolites reveals a wide pore-size distribution ranging from micro to macropores. As can be seen in Fig. 3, the total pore volume of ITQ-6 is much larger than that of ITQ-2 while at relative partial pressures below 0.6 (which account for micropores and mesopores with diameters below about 4.5 nm as calculated by the BJH formalism) ITQ-2 shows a higher adsorption capacity than ITQ-6. Then, it can be said that ITQ-2 possesses a large fraction of its porosity as micropores

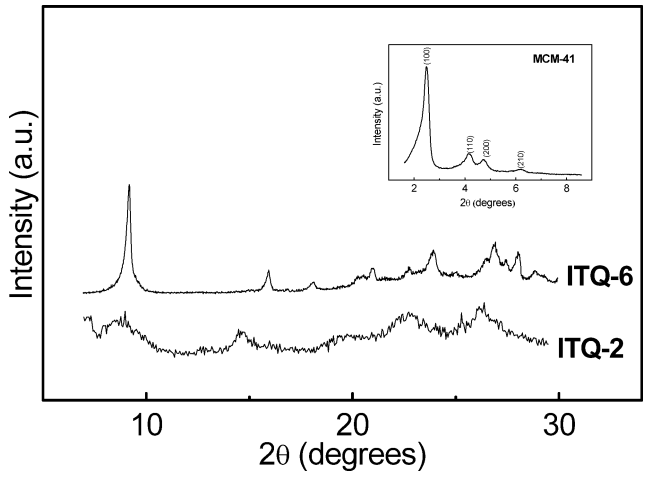

Fig. 2. X-ray diffraction patterns of calcined ITQ-2, ITQ-6, and MCM-41 (insert) materials.

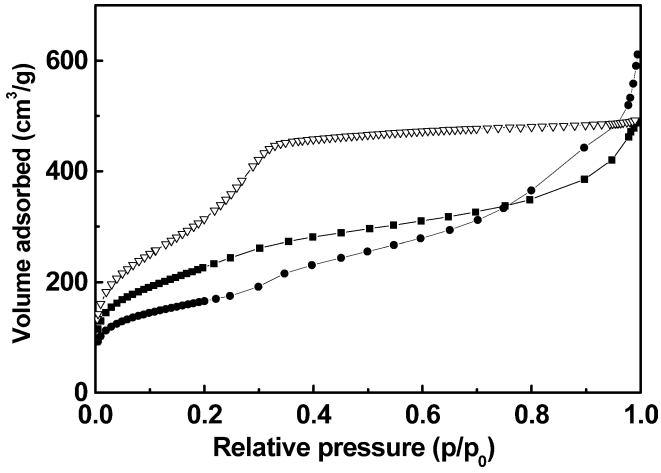

Fig. 3. Nitrogen adsorption isotherms of (■) ITQ-2, (●) ITQ-6, and (▽) MCM-41 samples.

and small mesopores while ITQ-6 has a larger contribution from macropores and large mesopores which are typically attributed to interparticular condensation [35]. These differences in porosity are probably the result of a distinct rearrangement of the layers in the two materials originated by the different structures and dimensions of the zeolitic layers in ITQ-2 and ITQ-6. Thus, the nitrogen adsorption results indicate that ITQ-6 contains a larger fraction of accessible external surface than ITQ-2.

The textural properties of the supports derived from the N_2 adsorption isotherms are summarized in Table 1. As observed, ITQ-2 presents a higher BET surface area (822 m^2/g) than ITQ-6 (585 m^2/g), though the latter has a larger pore volume. Both ITQ-2 and ITQ-6 zeolites show a much higher surface area and total pore volume than the amorphous silica sample. On the other hand, the pure silica mesoporous MCM-41 sample shows the highest surface area (1223 m^2/g).

The textural properties of the Co-containing catalysts are also given in Table 1. A reduction of surface area and pore

Table 1
Textural properties of supports and Co-containing catalysts determined by nitrogen adsorption

Sample	Co content (wt%)	Surface area (BET) (m^2/g)	Pore volume (BJH) (cm^3/g)	Average pore diameter (BJH) (nm)
ITQ-2	–	822	0.76	3.7
ITQ-6	–	585	0.94	6.4
MCM-41	–	1223	0.76	2.2
SiO_2	–	387	0.80	8.6
Co/ITQ-2	20.0	484	0.55	4.5
Co/ITQ-6	20.5	350	0.61	7.0
Co/MCM-41	19.3	711	0.44	2.3
Co/SiO_2	20.2	260	0.54	6.5

volume is noted for all catalysts after incorporation of cobalt (ca. 20 wt% Co). The decrease of surface area is mainly due to a "dilution" effect caused by the presence of the supported cobalt oxide phase. Nevertheless, the relative loss of surface area taking into account the dilution effect (assuming that cobalt in calcined samples is present in the form of Co_3O_4, as will be shown later, and that this phase does not contribute to the surface area) is about 20% for Co/ITQs and Co/MCM-41 catalysts, and ca. 10% for Co/SiO_2. This indicates that a partial plugging of the support pores has also occurred after Co incorporation. It is seen in Table 1 that Co/ITQs have a larger surface area than the conventional Co/SiO_2 catalyst. Furthermore, the ordered mesoporous structure of the MCM-41 support is preserved after Co loading, as indicated by the presence of the low-angle XRD peak (not shown) and the very high surface area ($> 700\ m^2/g$) of the Co/MCM-41 sample.

3.1.2. Cobalt structure and particle size

The X-ray diffractograms of the oxidized Co catalysts (not shown) exhibit the reflections at 2θ of about 31.3, 36.9, 45.0, 59.4, and 65.4° characteristic of the spinel Co_3O_4 phase, as it is usually observed for siliceous materials impregnated with cobalt nitrate precursor [21,22,25,27,36]. The average diameter and distribution of the supported cobalt particles in oxidized catalysts were investigated by TEM. As an example, bright-field and dark-field TEM images of Co/ITQ-6 are presented in Fig. 4. In the dark-field image (Fig. 4b) the cobalt nanoparticles clearly appear as bright spots. Direct observation of bright-field TEM images of the studied catalysts allows for obtaining the average size and distribution of the supported cobalt particles. The cobalt particle-size distributions obtained for the different catalysts are shown in Fig. 5. A pronounced maximum for particles of 6 nm diameter, representing about 24% of the total Co particles, is found in Co/ITQ-6. The maximum in the particle-size distribution is shifted toward larger diameters in Co/ITQ-2 (9 nm) and Co/SiO_2 (8 nm). The distribution of cobalt particles appears to be more heterogeneous in Co/SiO_2, while Co/ITQ-2 contains a larger proportion of particles in the 7–9 nm range. Higher differences in particle-size distribution are evident for Co/ITQ-6 catalyst, for which about 50%

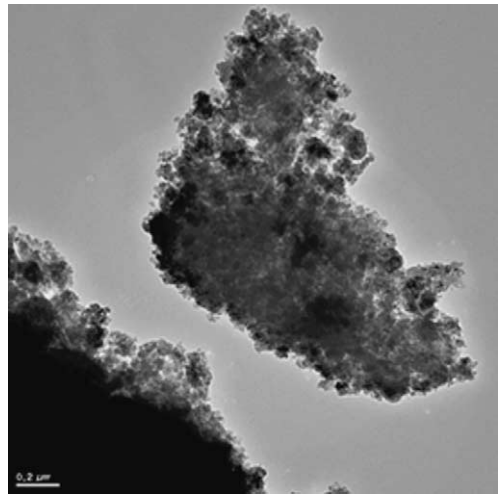

(a)

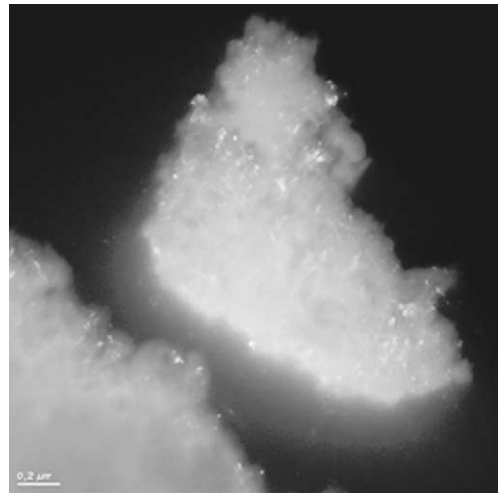

(b)

Fig. 4. Bright-field (a) and dark-field (b) TEM images of Co/ITQ-6 sample.

of the Co_3O_4 particles have a diameter below 7 nm. On the other hand, a clear bimodal distribution with a sharp maximum at 3 nm and a broader one centered at 19 nm is observed in the Co/MCM-41 sample. The first maximum mimics the mean diameter of the MCM-41 host (3.1 nm as determined by N_2 adsorption) and thus corresponds to Co_3O_4 particles encapsulated within the mesoporous channels, while the second maximum indicates the presence of larger cobalt particles deposited on the external surface.

The average particle size obtained from the above particle-size distributions and the corresponding Co^0 dispersions calculated as explained under Experimental are given in Table 2. As observed, the average diameter of Co_3O_4 crystallites in Co/MCM-41 (9.2 nm) and Co/ITQ-6 (9.3 nm) is lower than in Co/ITQ-2 (11.7 nm) and Co/SiO_2 (10.6 nm). For comparison purposes, the average diameters of the Co_3O_4 crystallites estimated from XRD patterns using the Scherrer equation [37] are also given in Table 2. Except for the Co/MCM-41 sample, XRD crystallite diameters are about 1.5 to 2.4 times larger than the corresponding TEM

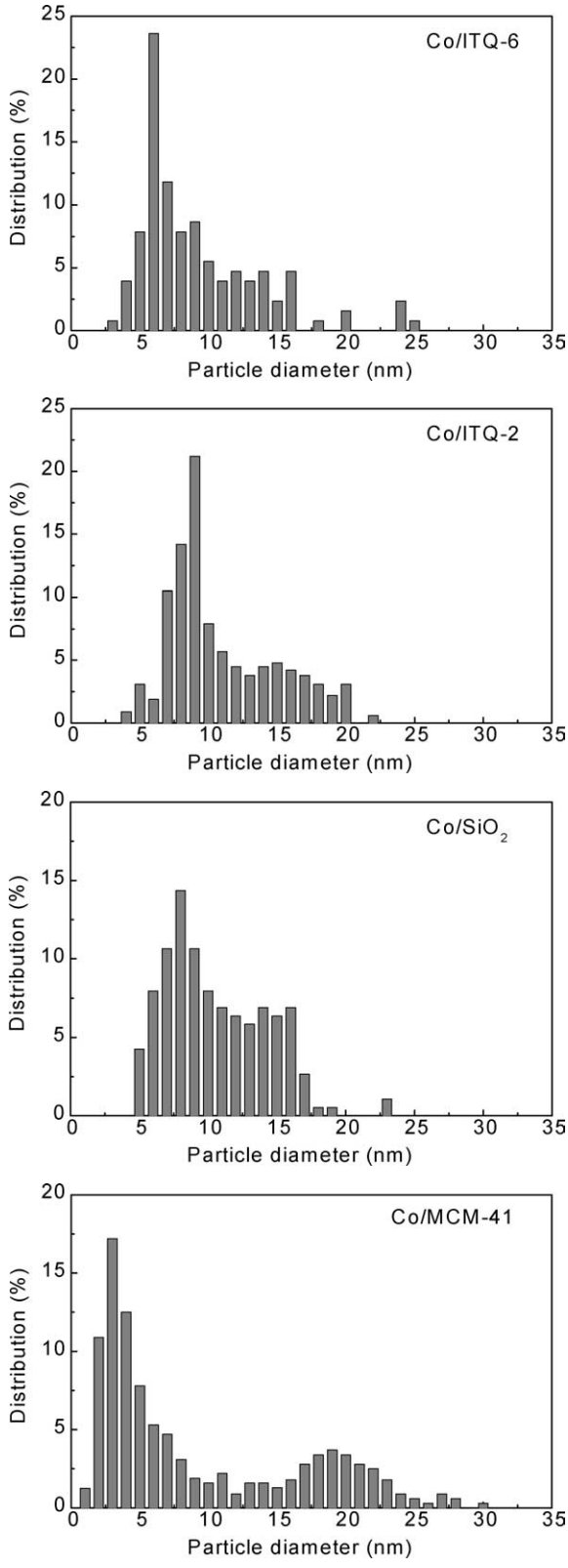

Fig. 5. Cobalt particle-size distributions as determined by TEM.

values. Usually, larger values have been reported for average particle sizes estimated from XRD as compared to other techniques [38,39]. These discrepancies have been explained by considering the limitations and approximations of using XRD line broadening, which generally tend to overstate the actual particle sizes.

Table 2
Average particle size, dispersion, and reducibility of the supported cobalt particles

Catalyst	TEM		XRD	Degree of reduction (%)
	D_p (Co_3O_4) (nm)	D (Co^0) (%)	D_p(Co_3O_4) (nm)	
Co/ITQ-2	11.7	10.9	17.3	89
Co/ITQ-6	9.3	13.8	20.9	88
Co/MCM-41	9.2	13.9	5.5	38
Co/SiO_2	10.6	12.1	15.6	96

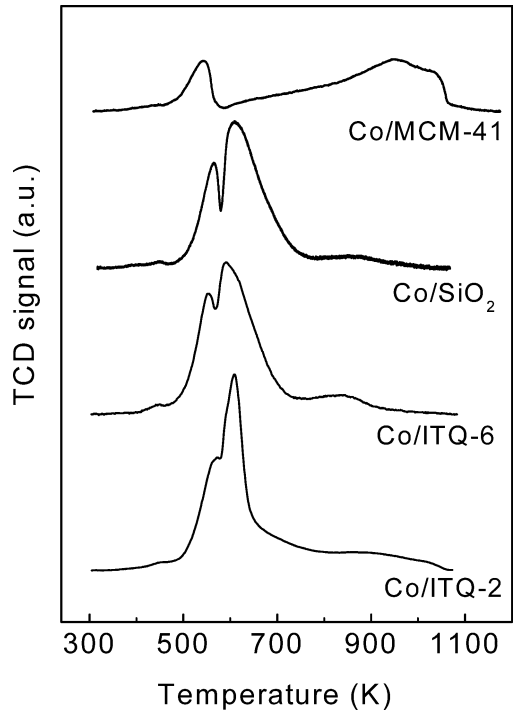

Fig. 6. TPR profiles of cobalt-supported catalysts.

3.1.3. Reducibility of the Co species

The reduction behavior of the supported cobalt oxide particles in the different supports has been studied by temperature-programmed reduction (TPR). The corresponding reduction curves are shown in Fig. 6. As observed, Co/ITQ and Co/SiO_2 catalysts exhibit two main reduction features with maxima at about 550–570 K and 600–620 K, which correspond to the two-step reduction process in which Co_3O_4 is first reduced to CoO and then CoO is reduced to Co^0, as reported by different authors [16,36,40,41]. The TPR profiles are quite similar for the delaminated and SiO_2-based catalysts, suggesting a comparable reducibility of the supported oxidic species. Nevertheless, Co/ITQ-6 shows a broad and small reduction feature in the range of 800–900 K that could be attributed to the reduction of the smaller cobalt particles (probably those with less than 5 nm in diameter)

detected by TEM and which were not observed on Co/ITQ-2 and Co/SiO_2. On the other hand, a quite different reduction pattern is found for Co/MCM-41. This sample shows a first reduction peak with a maximum at about 543 K, most likely corresponding to the reduction of the larger Co_3O_4 particles located on the external surface, as observed by TEM, and probably also to the contribution of partial reduction (Co_3O_4 to CoO) of the smaller particles. This sample also shows a second broad reduction feature at higher temperatures with maximum hydrogen consumption above 900 K, which are typical for the reduction of cobalt silicates probably formed by reaction of highly dispersed CoO with the silica support during the reduction process [27,36,42]. In the case of Co/MCM-41, the very small cobalt particles confined inside the mesoporous channels would favor the CoO-support interaction leading to the formation of hardly reducible cobalt species. A lower reducibility of small cobalt particles located in narrow pores of the support has also been related to a slower diffusion rate of the water formed in the reduction, increasing its residence time inside the pores [16,25,36].

The degrees of cobalt reduction determined by TPR after reducing the catalysts in hydrogen at 673 K for 10 h as explained under Experimental are given in Table 2. The values obtained are in good agreement with the TPR profiles discussed above. Thus, very high reduction degrees were obtained for Co/ITQs (88–89%) and Co/SiO_2 (96%), while the extent of reduction for Co/MCM-41 was only 38%. The slightly lower reduction degrees of Co/ITQs with respect to Co/SiO_2 may reflect the differences in particle-size distribution observed by TEM. It is worth noting the very high reducibility of cobalt oxides supported on ITQ-6, despite that this sample contains a larger proportion of small cobalt particles, as observed by TEM.

3.1.4. Nature of the cobalt species

IR spectroscopy of adsorbed CO has been extensively used to identify the nature of adsorption sites in cobalt catalysts [43–50]. The IR spectra of reduced Co/ITQ-6, Co/ITQ-2, and Co/SiO_2 samples at different CO coverage are shown in Figs. 7–9, respectively. As observed in Fig. 7, at low CO dosage Co/ITQ-6 displays a band at 2008 cm^{-1} with an asymmetry in the low frequency region. The asymmetry at low frequency may indicate the presence of another component at around 1960 cm^{-1}. Increasing the amount of adsorbed CO the band maximum at 2008 cm^{-1} is slightly shifted to higher frequencies (2013 cm^{-1}) while its intensity decreases and becomes more symmetric, suggesting a simultaneous decrease of the intensity of the low-frequency component at ca. 1960 cm^{-1}. In addition, a band at 1897 cm^{-1}, which increases in intensity at higher CO dosages, is clearly observed. This band appears to be stable towards evacuation, as observed in spectrum *d* (dotted line) in Fig. 7.

The IR spectra of CO adsorbed on Co/ITQ-2 (Fig. 8) also present, at low coverage, a band at 2006 cm^{-1} with a low-frequency tail at around 1945 cm^{-1}. The band at 2006 cm^{-1} is shifted to higher frequencies (2012 cm^{-1}) and decreases

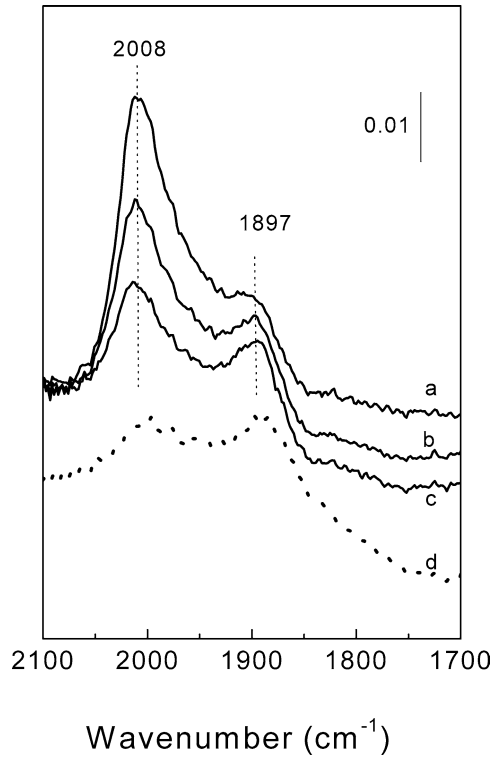

Fig. 7. FTIR spectra of CO adsorbed on Co/ITQ-6 at different CO dosages: (a) 13.4 mbar, (b) 47.5 mbar, (c) 135.3 mbar, (d) evacuation spectrum.

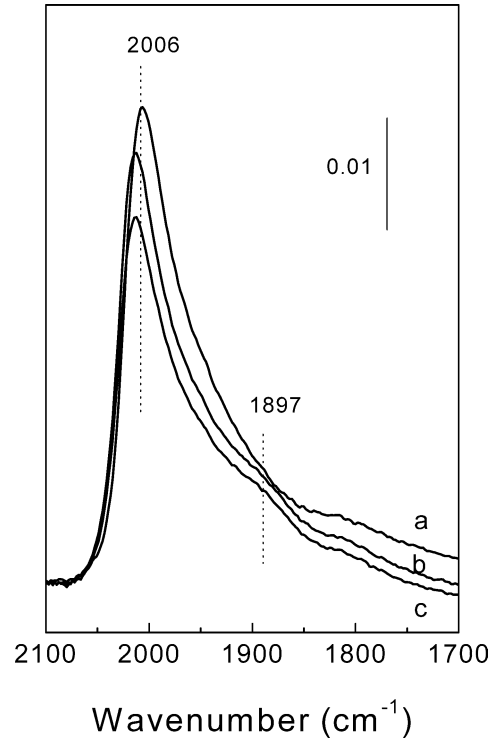

Fig. 8. FTIR spectra of CO adsorbed on Co/ITQ-2 at different CO dosages: (a) 6.2 mbar, (b) 54.3 mbar, (c) 71.1 mbar.

in intensity with increasing CO dosage, as it was also observed for Co/ITQ-6. However, the relative decrease in intensity of the 2006 cm^{-1} band is lower in Co/ITQ-2 than in

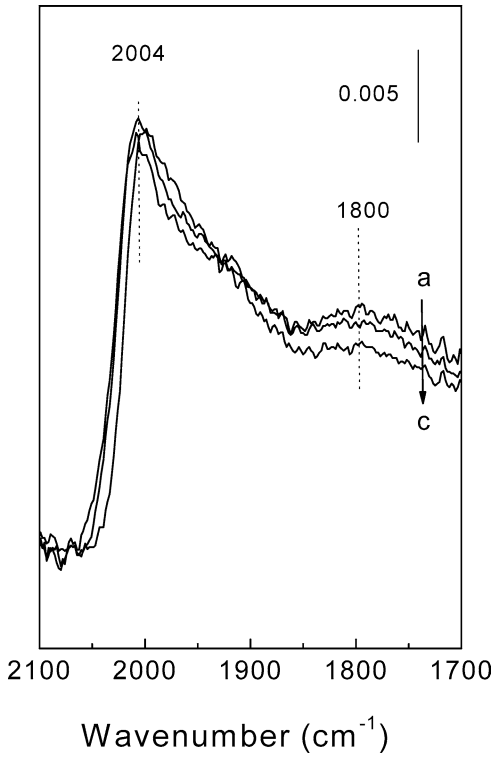

Fig. 9. FTIR spectra of CO adsorbed on Co/SiO_2 at different CO dosages: (a) 3.5 mbar, (b) 57.0 mbar, (c) 130.0 mbar.

Co/ITQ-6. In addition, the band at 1897 cm^{-1} is also evidenced in Fig. 8, especially at higher CO coverage, though its relative intensity is lower than in Co/ITQ-6. Moreover, a low intense band at around 1800 cm^{-1} is observed in the spectra of Co/ITQ-2.

The IR spectra of Co/SiO_2 (Fig. 9) at low CO dosage presents an intense band at 2004 cm^{-1} with a broad shoulder around 1930 cm^{-1}. Increasing CO dosage shifts the 2004 cm^{-1} band to higher frequencies (2007 cm^{-1}) but, contrary to what was found in Co/ITQ-6 and Co/ITQ-2 samples, its intensity hardly changes with increasing CO dosage. The broadness of the low-frequency tail suggest heterogeneity of cobalt adsorption sites that could be related to the heterogeneous particle-size distribution observed by TEM. Furthermore, a band at about 1800 cm^{-1} is also observed in Co/SiO_2, the relative intensity of which is higher than in the delaminated catalysts (it is hardly visible in Co/ITQ-6). The presence of the adsorption band at 1897 cm^{-1} cannot be completely neglected in the spectra of Co/SiO_2 due to the broad low-frequency shoulder but if present, its intensity should be significantly lower than in Co/ITQ-6 and Co/ITQ-2.

It is worth noting the absence of CO adsorption bands above 2100 cm^{-1} in the IR spectra of the three catalysts studied, indicating that oxidized cobalt species ($CO–Co^{n+}$) should be, if any, in very low amounts [48]. This is in agreement with the very high reducibility of these catalysts observed by TPR experiments.

The IR band in the 2010–2000 cm^{-1} region observed in the IR spectra of the three catalysts investigated has been unambiguously assigned to CO linearly adsorbed on cobalt metal [48–50]. The blue shift of the band maximum with increasing CO coverage is attributed to dipole–dipole interaction effects of adsorbed CO molecules. On the other hand, the assignation of the IR bands at lower frequencies (< 2000 cm^{-1}) is still a matter of controversy in the literature. Thus, polycarbonyl $Co(CO)_x$ $(x > 1)$ species [48], bridged-type CO species [48, and references therein, 49, 50], and CO linearly adsorbed on coordinatively unsaturated metal sites [51–53] have been postulated by different authors. Polycarbonyl species are unlikely to form at low CO coverage and they are less stable toward evacuation, in contrast to what is found for the 1897 cm^{-1} band. In addition, no bands are observed in the region between 1800 and 1700 cm^{-1} which is the typical region for vibrations of polycarbonyl species [48]. On the other hand, our TEM results do not support the assignment of the 1897 cm^{-1} band to bridged-type CO species. Indeed, bridged CO species are preferentially formed on flat metal surfaces associated with larger cobalt particles [48,54,55], whereas the intensity of the 1897 cm^{-1} band is higher in Co/ITQ-6 having a greater proportion of smaller cobalt particles. Therefore, we tentatively ascribe this band to CO linearly adsorbed on coordinatively unsaturated cobalt metal sites, such as those located in edges, corners, and dislocations, which would be more abundant in smaller crystallites. This type of site will show a high density of d-electrons favoring the backdonation of electrons to the $2\pi^*$ antibonding molecular orbital of CO, with a consequent reduction in vibrational frequency. In fact, theoretical calculations have predicted bands at 1867, 1907, and 1835 cm^{-1} for cobalt atoms on edges and on two different types of corners, respectively [45]. Finally, the band in the lower frequency region at ca. 1800 cm^{-1} observed in Co/ITQ-2 and Co/SiO_2 is usually assigned to CO adsorbed on multifold metal cobalt sites [49,56].

Worth noting is the decrease of the intensity of the IR bands at about 2000–2010 cm^{-1} and 1960–1930 cm^{-1} with increasing CO dosage in Co/ITQ-6 and, to a lesser extent, in Co/ITQ-2 samples. Such a decrease of intensity of the IR-CO bands can be attributed to dissociation and/or disproportionation of CO on the metal surface [45,48]. Actually, a band at 1615 cm^{-1} related to surface carbonate species [50] develops in Co/ITQ-6 at increasing CO coverage (not shown), suggesting that CO_2 was formed by disproportionation of CO. The band at about 1615 cm^{-1} is also evidenced in the IR spectrum of Co/ITQ-2, though in a lower intensity than in Co/ITQ-6, and is hardly observed in Co/SiO_2, in close agreement with the relative decrease in intensity of the 2000–2010 cm^{-1} band upon increasing CO dosage observed for the three catalysts studied. At the present time, we do not have a plausible explanation for the higher reactivity of the cobalt sites in Co/ITQ-6 (and to a lesser extent in Co/ITQ-2) toward CO dissociation/disproportionation, and

Table 3
Catalytic results for the FTS reaction on Co-supported catalysts

Catalyst	CO conv. (%)	Reaction rate (10^{-3} s^{-1})	TOF[a] (10^{-2} s^{-1})	Hydrocarbon distribution (%C)			α[b]
				C_1	C_2–C_4	C_{5+}	
Co/ITQ-6	37.5	5.51	4.5	10.7	11.0	78.3	0.85
Co/ITQ-2	21.9	3.30	3.4	13.2	14.2	72.6	0.83
Co/MCM-41	24.3	3.80	7.2	25.6	29.7	44.7	0.76
Co/SiO_2	20.2	3.01	2.6	16.6	17.9	65.5	0.81

Reaction conditions: $T = 493$ K, $P = 20$ bar, $H_2/CO = 2$, GHSV = 13.5 $L_{syngas}/(g_{cat}\ h)$.

[a] Turnover frequencies estimated from the TEM Co^0 dispersions and the degrees of reduction.

[b] Chain growth probability obtained from the ASF plot in the C_1–C_{20} hydrocarbon range.

further spectroscopic work is in progress to elucidate this effect.

3.2. Fischer–Tropsch synthesis results

The FTS catalytic performance of the different Co-supported catalysts was evaluated in a fixed-bed reactor under typical hydrocarbon synthesis conditions: 493 K, 20 bar, $H_2/CO = 2$, and GSHV of 13.5 $L_{syngas}/(g_{cat}\ h)$. The activity and selectivity results corresponding to the pseudo-stationary period (15–20 h on stream) are presented in Table 3. As observed, the Co/ITQ-6 catalyst displays a much higher CO conversion than the rest of catalysts tested. The global reaction rates calculated as the moles of CO converted per mole of total cobalt and per second are also included in Table 3. The FTS reaction rate of Co/ITQ-6 is about 1.5 and 1.8 times greater than that of Co/MCM-41 and Co/SiO_2, respectively. On the other hand, Co/ITQ-2 gives a reaction rate which is slightly higher (1.1) than that of Co/SiO_2. In the case of Co/MCM-41 the relatively low activity can be ascribed to the poor reducibility of the very small Co particles confined within the mesoporous channels. By contrast, the high activity of Co/ITQ-6 originates from its relatively low Co particle size and its high reduction degree, resulting in a greater density of active surface Co^0 sites. From a practical point of view, these results show that by using the delaminated ITQ-6 zeolite having a high external surface area one can achieve FTS activity per mass of cobalt that is significantly higher than that of catalysts based on ordered mesoporous silicas and conventional amorphous silica.

In principle, one might expect the FTS activity to be proportional to the concentration of surface cobalt metal sites (Co^0_S), that is, the intrinsic activity (turnover) of the accessible Co^0 sites should be constant. The TOF values estimated from the TEM Co^0 dispersions and the degrees of reduction are given in Table 3. Turnover frequencies appear to be similar for Co/ITQs and Co/SiO_2 (ranging from 2.6 for Co/SiO_2 to 4.5 for Co/ITQ-6), while a slightly higher value (7.2) is obtained for Co/MCM-41. It must be taken into account that these values are exposed to some uncertainty as the Co^0 dispersions in reduced catalysts are estimated from the TEM Co_3O_4 dispersions in oxidized samples, as explained under Experimental. Breakup of the supported cobalt particles might occur during the reduction process that would lead to an underestimation of the Co^0 dispersion. Moreover, differences in the accessibility to the active Co^0 sites might also lead to changes in the apparent TOF values for the different catalysts. Taking all this into consideration, it becomes clear that several factors may contribute to the differences in TOF shown in Table 3.

On the other hand, distinct hydrocarbon selectivities are found for the different catalysts. As observed in Table 3, the mesoporous Co/MCM-41 catalyst gives the highest selectivity to methane (25.6%) and the lowest selectivity to C_{5+} hydrocarbons (44.7%). A high methane selectivity is usually reported for catalysts having high metal dispersion and low Co reducibility [14,20], as is the case of Co/MCM-41. In fact, Khodakov et al. [22] found an inverse relationship between the methane selectivity and the extent of overall reduction for cobalt-supported mesoporous silicas. The higher methanation activity of Co/MCM-41 may thus be responsible for its low C_{5+} selectivity. By contrast, Co/ITQ-6 gives the highest selectivity to C_{5+} hydrocarbons (78.3%), followed by Co/ITQ-2 (ca. 72.6%), and Co/SiO_2 (ca. 65.6%). The chain growth probability (α) obtained from the Anderson–Shultz–Flory (ASF) plots in the C_1–C_{20} hydrocarbon range is 0.85 for Co/ITQ-6, 0.83 for Co/ITQ-2, 0.81 for Co/SiO_2, and 0.76 for Co/MCM-41, thus reflecting the enhanced formation of heavier hydrocarbons in the delaminated catalysts.

It is well known that FTS selectivities may be affected by conversion, and therefore, they should be compared at similar conversion levels to assess any changes arising from differences in catalyst properties. In general, one would expect the C_{5+} selectivity to increase with increasing the CO conversion. Then, it is clear from the results presented in Table 3 that the lower C_{5+} selectivity obtained for Co/MCM-41 at a higher conversion as compared with Co/SiO_2 is ascribed to the particular properties (i.e., high dispersion and low reducibility) of the Co particles supported on the mesoporous material. Furthermore, the superior C_{5+} selectivity of Co/ITQ-2 with respect to Co/SiO_2 should reflect differences in catalyst properties, as both catalysts display very close conversion levels (21.9 and 20.2%, respectively). However, this is not the case of Co/ITQ-6 which shows a CO conversion significantly higher (37.5%) than the rest of catalysts studied. In order to separate the effect of conversion from the selectivity data given in Table 3, the Co/ITQ-6 cat-

Table 4
Influence of conversion on hydrocarbon selectivities for Co/ITQ-6 catalyst

CO conversion (%)	Hydrocarbon distribution (%C)		
	C_1	C_2–C_4	C_{5+}
37.5	10.7	11.0	78.3
30.4	13.5	12.6	73.9
24.3	15.4	12.4	72.2
19.6	16.4	11.8	71.8

Reaction conditions: $T = 493$ K, $P = 20$ bar, $H_2/CO = 2$, GHSV = 13.5–27 $L_{syngas}/(g_{cat}\,h)$.

alyst was evaluated at different space velocities ranging from 13.5 to 27.0 $L_{syngas}/(g_{cat}\,h)$ while keeping constant the rest of conditions. The hydrocarbon selectivities obtained at different conversion levels over Co/ITQ-6 are shown in Table 4. As expected, the C_{5+} selectivity decreases with decreasing CO conversion while the selectivity to methane follows the opposite trend. As seen in Table 4, a C_{5+} selectivity of ca. 72% is obtained for Co/ITQ-6 at a conversion of about 20%, which is very close to that of Co/ITQ-2 and still higher than that of Co/SiO_2 at the same conversion level. These results clearly indicate that the superior C_{5+} selectivity obtained for Co/ITQ-6 and Co/ITQ-2 catalysts must be ascribed to the particular properties of the Co particles supported in the delaminated zeolites.

The chain growth probability during Fischer–Tropsch synthesis on supported cobalt catalysts generally increases with the size of the reduced Co particles [14,21,27,57] up to a certain particle size above which it remains invariant [12,58]. According to the model proposed by Iglesia [13], this effect can be explained in terms of a diffusion-enhanced readsorption of the primary α-olefins which could thus participate in the chain-growing processes favoring the formation of longer hydrocarbon chains. In our case, the increased C_{5+} selectivity observed over Co/ITQ-6 and Co/ITQ-2 as compared to Co/SiO_2 cannot be attributed to the presence of larger cobalt particles in the former catalysts which, according to TEM results, contained a higher proportion of cobalt particles of smaller diameter. On the other hand, both Co/ITQ-2 and Co/ITQ-6 were seen to present an intense band at 1897 cm^{-1} in the infrared spectra that we attributed to CO linearly adsorbed on coordinatively unsaturated cobalt metal sites, such as those located in edges and/or corner positions of the crystallites. Besides the differences in particle-size distribution observed by TEM, changes in the morphology of the crystallites induced by the particular porosity of the delaminated zeolites might also contribute to the higher concentration of low coordinated centers in Co/ITQ-6 catalyst (and to a lesser extent in Co/ITQ-2) as compared with Co/SiO_2. In this respect, Schulz et al. [59] observed an increase of the chain growth probability during the initial stages of the FTS reaction and proposed that the formation of higher hydrocarbons would be favored on low coordination cobalt centers formed in this stage by segregation of larger cobalt particles. Then, we can suggest that the higher concentration of coordinatively unsaturated cobalt metal sites (giving a CO adsorption band at 1897 cm^{-1}) may be responsible for the higher C_{5+} selectivity observed in Co/ITQ-6 and Co/ITQ-2 as compared with Co/SiO_2. This type of site having several free valences might stabilize the surface hydrocarbon intermediates formed during the Fischer–Tropsch reaction favoring the hydrocarbon chain growth by successive insertions of monomeric $–CH_x–$ species.

4. Conclusions

In this work we have applied all-silica ITQ-2 and ITQ-6 delaminated materials having a high external surface area (> 500 m^2/g) as supports for preparing cobalt-based Fischer–Tropsch catalysts. The spinel Co_3O_4 is the only crystalline cobalt phase detected by XRD in calcined Co/ITQ catalysts (ca. 20 wt% Co content). The supported Co_3O_4 particles are better dispersed on ITQ-6 having a very large and accessible external surface as compared with ITQ-2 and amorphous SiO_2. According to TEM measurements, Co/ITQ-6 contains a greater proportion of relatively small cobalt particles with a pronounced maximum in the particle-size distribution at 6 nm representing about 24% of the total particles. Thus, the average cobalt particle size in Co/ITQ-6 (9.3 nm) is lower than in Co/ITQ-2 (11.7 nm) and Co/SiO_2 (10.6 nm). It is remarkable that, despite the relatively high proportion of small particles, the reducibility of Co/ITQ-6 catalyst is very high. Thus, about 90% of the Co_3O_4 particles in Co/ITQ-6 are reduced to metallic cobalt after hydrogen treatment at 673 K, which is comparable to the reduction degrees obtained for Co/ITQ-2 and Co/SiO_2 having larger cobalt particles. The mesoporous Co/MCM-41 sample displays a bimodal distribution of cobalt particles with maxima at 3 and 19 nm diameters corresponding to particles confined within the mesopores (3.1 nm diameter) and on the external surface, respectively. The average particle size obtained from this distribution is 9.2 nm, very close to that of Co/ITQ-6. However, contrary to Co/ITQ-6, the cobalt reducibility in Co/MCM-41 is much lower (38% reduction degree) which is ascribed to a strong Co–support interaction of the very small particles confined within the mesoporous channels. The relatively good cobalt dispersion and high reducibility achieved on ITQ-6 result in a highly active catalyst for the Fischer–Tropsch synthesis reaction. Thus, Co/ITQ-6 displays a CO hydrogenation rate about 1.8 and 1.5 times higher than that of Co/SiO_2 and Co/MCM-41. The reaction rate of Co/ITQ-2 is only slightly higher than that of Co/SiO_2. Moreover, the catalysts based on ITQ-6 and ITQ-2 give the highest selectivity to long-chain (C_{5+}) hydrocarbons. We ascribe the higher C_{5+} selectivity of these catalysts to a higher concentration of coordinatively unsaturated Co^0 centers, which are characterized by a band at 1897 cm^{-1} in the infrared spectra of adsorbed CO. This type of site having an enhanced electron density might stabilize surface hydrocarbon intermediates favoring chain growth processes.

Acknowledgments

Financial support by the Comisión Interministerial de Ciencia y Tecnología (CICYT) of Spain (Project MAT2001-2726) is gratefully acknowledged. C. López acknowledges the Ministerio de Ciencia y Tecnología of Spain for a Ph.D. scholarship. We also thank Prof. A. Corma, Prof. V. Fornés, and Dr. F. Rey for their helpful discussions.

References

[1] J.H. Gregor, Catal. Lett. 7 (1990) 317.
[2] M.E. Dry, J. Chem. Technol. Biotechnol. 77 (2001) 43.
[3] H. Schulz, Appl. Catal. A 186 (1999) 3.
[4] D.J. Duvenhage, T. Shingles, Catal. Today 71 (2002) 301.
[5] S.T. Sie, R. Krishna, Appl. Catal. A 186 (1999) 55.
[6] M.E. Dry, Catal. Today 71 (2002) 227.
[7] M.E. Dry, J. Chem. Technol. Biotechnol. 77 (2001) 43.
[8] P.J. Van Berge, S. Barradas, J. Van de Loodsrecht, J.L. Visage, Petrochemie (2001) 138.
[9] T.H. Fleisch, R.A. Sills, M.D. Briscoe, J. Nat. Gas. Chem. 11 (2002) 1.
[10] P.J. Van Berge, S. Barradas, J. Van De Loodsrecht, J.L. Visagie, Erdoel, Erdgas, Kohle 117 (2001) 138.
[11] R. Oukaci, A.H. Singleton, J.G. Goodwin Jr., Appl. Catal. A 186 (1999) 129.
[12] E. Iglesia, S.L. Soled, R.A. Fiato, J. Catal. 137 (1992) 212.
[13] E. Iglesia, Appl. Catal. A 161 (1997) 59.
[14] R.C. Reuel, C.H. Bartholomew, J. Catal. 85 (1984) 78.
[15] B.G. Johnson, C.H. Bartholomew, D.W. Goodman, J. Catal. 128 (1991) 231.
[16] R. Riva, H. Miesner, R. Vitali, G. Del Piero, Appl. Catal. A 196 (2000) 111.
[17] G. Jacobs, T.K. Das, Y. Zhang, J. Li, G. Racoillet, B.H. Davis, Appl. Catal. A 233 (2002) 263.
[18] N. Tsubaki, S. Sun, K. Fujimoto, J. Catal. 189 (2001) 236.
[19] E. Iglesia, S.L. Soled, R.A. Fiato, G.H. Via, Stud. Surf. Sci. Catal. 81 (1994) 433.
[20] A. Martínez, C. López, F. Márquez, I. Díaz, J. Catal. 220 (2003) 486.
[21] A.Y. Khodakov, A. Griboval-Constant, R. Bechara, F. Villain, J. Phys. Chem. B 105 (2001) 9805.
[22] A. Khodakov, A. Griboval-Constant, R. Bechara, V.L. Zholobenko, J. Catal. 206 (2002) 230.
[23] D. Yin, W. Li, W. Yang, H. Xiang, Y. Sun, B. Zhong, S. Peng, Micropor. Mesopor. Mater. 47 (2001) 15.
[24] S. Suvato, T.A. Pakkanen, J. Mol. Catal. A: Chem. 164 (2000) 273.
[25] J. Panpranot, J.G. Goodwing Jr., A. Sayari, Catal. Today 77 (2002) 269.
[26] A.Y. Khodakov, R. Bechara, A. Griboval-Constant, Appl. Catal. A 254 (2003) 273.
[27] A.M. Saib, M. Claeys, E. van Steen, Catal. Today 71 (2002) 395.
[28] A. Corma, U. Diaz, M.E. Domine, V. Fornés, Angew. Chem. Int. Ed. 39 (8) (2000) 1499.
[29] A. Corma, V. Fornés, S.B. Pergher, patent EP 9605004, 1996, and WO 9717290, 1997.
[30] A. Corma, V. Fornés, J. Martínez-Triguero, S.B. Pergher, J. Catal. 186 (1999) 57.
[31] A. Corma, A. Martínez, V. Martinez-Soria, J. Catal. 200 (2) (2001) 259.
[32] A. Corma, Q. Kan, M.T. Navarro, J. Pérez-Pariente, Chem. Mater. 9 (1997) 2123.
[33] R.D. Jones, C.H. Bartholomew, Appl. Catal. 39 (1988) 77.
[34] R.C. Reuel, C.H. Bartholomew, J. Catal. 85 (1984) 63.
[35] S.J. Gregg, K.S.W. Sing, Adsorption, Surface Area and Porosity, Academic Press, 1982.
[36] B. Ernst, S. Libs, P. Chaumette, A. Kiennermann, Appl. Catal. A 186 (1999) 145.
[37] B.D. Cullity, Elements of X-Ray Diffraction, Addison–Wesley, London, 1878.
[38] D.G. Castner, P.R. Watson, I.Y. Chan, J. Phys. Chem. 93 (1989) 3188.
[39] Ganesan, H.K. Kuo, A. Saavedra, R.J. De Angelis, J. Catal. 52 (1978) 319.
[40] A.Y. Khodakov, J. Lynch, D. Bazin, B. Rebours, N. Zanier, B. Moisson, P. Chaumette, J. Catal. 168 (1997) 16.
[41] D.G. Castner, P.R. Watson, I.Y. Chang, J. Phys. Chem. 94 (1990) 819.
[42] B. Sexton, A. Hughes, T. Turney, J. Catal. 97 (1986) 390.
[43] J.A. Timmey, Inorg. Chem. 18 (1979) 2502.
[44] L.E.S. Rygh, O.H. Ellestad, P. Klaeboe, C.J. Nielsen, Phys. Chem. Chem. Phys. 2 (2000) 1835.
[45] L.E.S. Rygh, C.J. Nielsen, J. Catal. 194 (2000) 401.
[46] J. Wijtezak, R. Queau, R. Poilblanc, J. Catal. 37 (1975) 391.
[47] A.A. Khassin, T.M. Yurieva, V.V. Kaichev, V.I. Bukhtiyarov, A.A. Budneva, E.A. Paukshtis, V.N. Parmon, J. Mol. Catal. A 175 (2001) 189.
[48] M. Jiang, N. Koizumi, T. Ozaki, M. Yamada, Appl. Catal. A 209 (2001) 59.
[49] S. Sun, N. Tsubaki, K. Fujimoto, Appl. Catal. A 202 (2000) 121.
[50] S.-W. Ho, J. Catal. 175 (1998) 139.
[51] R. Queau, R. Poilblanc, J. Catal. 27 (1972) 200.
[52] G. Blyholder, M.C. Allen, J. Am. Chem. Soc. 91 (1969) 3159.
[53] J. Ansorge, H. Foerster, J. Catal. 68 (1981) 182.
[54] L.L. Sheu, Z. Karpinski, W.M.H. Sachtler, J. Phys. Chem. 93 (1989) 4890.
[55] O. Dulaurent, K. Chandes, C. Bouly, D. Bianchi, J. Catal. 188 (1999) 237.
[56] S. Ischi, Y. Ohno, B. Viswanathan, Surf. Sci. 161 (1985) 349.
[57] C.H. Bartholomew, Catal. Lett. 7 (1990) 27.
[58] A. Barbier, A. Tuel, I. Arcon, A. Kodre, G.A. Martin, J. Catal. 200 (2001) 106.
[59] H. Schulz, Z. Nie, F. Ousmanov, Catal. Today 71 (2002) 351.